

Third-generation muffin-tin orbitals

O. K. Andersen, T. Saha-Dasgupta*, S. Ezhov

Max-Planck Institut für Festkörperforschung, D-70569, Stuttgart, Germany

*S.N. Bose Centre, Kolkata 98, India

November 1, 2018

Abstract

By the example of sp^3 -bonded semiconductors, we illustrate what 3rd-generation muffin-tin orbitals (MTOs) are. We demonstrate that they can be downfolded to smaller and smaller basis sets: sp^3d^{10} , sp^3 , and bond orbitals. For isolated bands, it is possible to generate Wannier functions *a priori*. Also for bands, which overlap other bands, Wannier-like MTOs can be generated *a priori*. Hence, MTOs have a unique capability for providing chemical understanding.

Keywords. Band structure; density functional; LMTO; Wannier functions.

1 Introduction

Muffin-tin orbitals (MTOs) have been used for a long time in *ab initio*, *e.g.* density-functional (DF), calculations of the electronic structure of condensed matter. Over the years, several MTO-based methods have been developed. The ultimate aim is to find a generally applicable electronic-structure method which is *intelligible*, *fast*, and *accurate*.

In order to be *intelligible*, an electronic-structure method must employ a *minimal* and *flexible* basis of *short-ranged* orbitals. As an example, the method should be able to describe the valence band and the lower part of the conduction band in sp^3 -bonded materials using merely four short-ranged *s*- and *p*-orbitals per atom and, for insulating phases, using merely occupied orbitals such as bond orbitals. Another example is materials with strong electronic correlations. For such materials, one must first construct a small, but realistic Hilbert space of many-electron wave functions, and this requires an accurate and flexible single-particle basis of atom-centered short-ranged orbitals. A small basis of short-ranged orbitals is a prerequisite for a method to be intelligible and *fast*, but it may be a hindrance for its *accuracy*, because the orbitals of a smaller basis tend to be more complicated than those of a larger basis.

Most other density-functional methods, such as plane-wave pseudopotential, LAPW, PAW, and LCAO methods, aim at *simulation*, and are therefore primarily *accurate* and *robust*. But they are neither fast nor intelligible in the above-mentioned sense, because they employ basis sets with of order hundred functions per atom. With such methods, *understanding* can therefore only be attempted *after* the calculation, by means of projections onto *e.g.* Wannier functions in case of insulators, charge densities, electron-localization functions (ELFs), partial waves, a.s.o..

The so-called 3rd-generation MTO method (Andersen *et al* 1994, Andersen *et al* 1998, Andersen *et al* 2000, Tank and Arcangeli 2000, Andersen and Saha-Dasgupta 2000) should come close to what we have been aiming for. In the present paper we shall explain what 3rd-generation MTOs are and what they achieve. Emphasis will be on the so-called *downfolding* and *energy-mesh* features which enable MTO bases to be small, flexible, and accurate, as we shall demonstrate by exposing them to the above-mentioned sp^3 -test. From the result, the idea emerges, that for *band insulators*, an MTO basis can be designed *a priori* to span the Hilbert space of the

occupied states only. That is, there is one, and only one, such MTO per electron. To get this count right, one may associate each orbital with a nominal electron (or pair), and leave it to the method to *shape* the orbitals in such a way that the basis set becomes complete for the occupied states. This can be done because MTOs are *selective in energy*, in the sense that the MTOs of order N (NMTOs) are shaped in such a way that the NMTO basis set solves Schrödinger's equation *exactly* for $N+1$ single-particle energies, which in the present case must be chosen in such a way that they span the valence band. This ability to generate Wannier functions directly in real space, should be useful for *ab initio* molecular-dynamics simulations. NMTOs may also prove useful for designing many-electron wave functions, which describe correlated electron systems in a realistic way. The description of spin and orbital ordering is a trivial example. Also for the conduction bands of *metals*, Wannier-like, low-energy MTOs can be designed *a priori*. This has been demonstrated in several cases (Müller *et al* 1998, Sarma and Saha-Dasgupta 2000, Korotin 2000, Valenti *et al* 2001, Dasgupta *et al* 2002), most recently for the hole-doped cuprate high-temperature superconductors, where the material-dependent trend of the hopping integrals and their correlation with the maximum T_c was discovered (Pavarini *et al* 2001, Dasgupta *et al*).

For a description of how we expand the charge density locally in such a way that Poisson's equation can be solved and the total energy and forces can be evaluated fast and accurately, we refer to previous (Andersen *et al* 2000, Tank and Arcangeli 2000) and coming publications (Arcangeli and Andersen, Savrasov and Andersen). This part of the 3rd-generation computer code is still under construction.

2 Screened spherical waves, kinked partial waves, and muffin-tin orbitals

The 3rd-generation MTO formalism is the multiple-scattering – or KKR (Korringa 1947, Kohn and Rostoker 1954)– formalism for finding the solutions, $\Psi_i(\mathbf{r})$, of Schrödinger's equation for an electron in a muffin-tin potential, $V(\mathbf{r}) = \sum_R v_R(r_R)$, with the following three extensions:

1.: The KKR formalism is proved to hold, not only for superpositions of spherically-symmetric, non-overlapping potential wells, $v_R(r_R)$, but also to leading order in the potential-*overlap* (Andersen *et al* 1992). Here, and in the following, $r_R \equiv |\mathbf{r} - \mathbf{R}|$, and \mathbf{R} are the sites which we label by R . The potential, $v_R(r)$, is taken to vanish outside a radius, s_R , which should not exceed 1.6 times the radius of touching spheres. *i.e.*: $s_R + s_{R'} \lesssim 1.6 |\mathbf{R} - \mathbf{R}'|$ for any pair of sites, R and R' .

2.: Exact *screening* transformations of the spherical waves, $n_l(\kappa r_R) Y_L(\hat{r}_R)$, are introduced in order to reduce the spatial range and the energy dependence ($\kappa^2 \equiv \varepsilon$) of the wave-equation solutions, $\psi_{RL}(\varepsilon, \mathbf{r})$ (Andersen and Jepsen 1984, Andersen *et al* 1992, Zeller *et al* 1995). Here, and in the following, $L \equiv lm$ labels the spherical- (or cubic-) harmonic's character.

3.: Energy-independent MTO basis sets are derived which span the solutions $\Psi_i(\mathbf{r})$ with energies ε_i of Schrödinger's equation to within errors proportional to $(\varepsilon_i - \varepsilon_0)(\varepsilon_i - \varepsilon_1) \dots (\varepsilon_i - \varepsilon_N)$, where $\varepsilon_0, \varepsilon_1, \dots, \varepsilon_N$ is a chosen *energy mesh* with $N+1$ points (Andersen *et al* 2000, Andersen and Saha-Dasgupta 2000). Such an energy-independent set of N th-order MTOs is called an NMTO set. By virtue of the variational principle, the errors of the energies ε_i will be proportional to $(\varepsilon_i - \varepsilon_0)^2 (\varepsilon_i - \varepsilon_1)^2 \dots (\varepsilon_i - \varepsilon_N)^2$.

At the top of figure 1 we show the LDA energy bands $\varepsilon_i(\mathbf{k})$ of Si in the diamond structure, calculated with the basis set of Si-centered *s*-, *p*-, and *d*-MTOs, *i.e.* with 9 orbitals/atom, for the 3-point energy mesh $\varepsilon_0, \varepsilon_1, \varepsilon_2$ indicated on the right-hand side. These bands have meV-accuracy for the MT-potential, which in the present case was the standard all-electron DF-LDA atomic-spheres potential. Since three energy points were used, the MTOs are of order $N=2$, that is, they are quadratic MTOs, so-called QMTOs.

The QMTO, $\chi_{p_{111}}^{(2)}(\mathbf{r})$, pointing along $[111]$ from one Si to its nearest neighbor, is shown in the $(2\bar{1}\bar{1})$ -plane by the first contour plot. This orbital is localized and smooth, with a few "orthogonality wiggles" at the nearest neighbor. The remaining three contour plots show major constituents of this p_{111} -QMTO: The p_{111} -kinked partial wave (KPW), $\phi_{p_{111}}(\epsilon, \mathbf{r})$, at the central

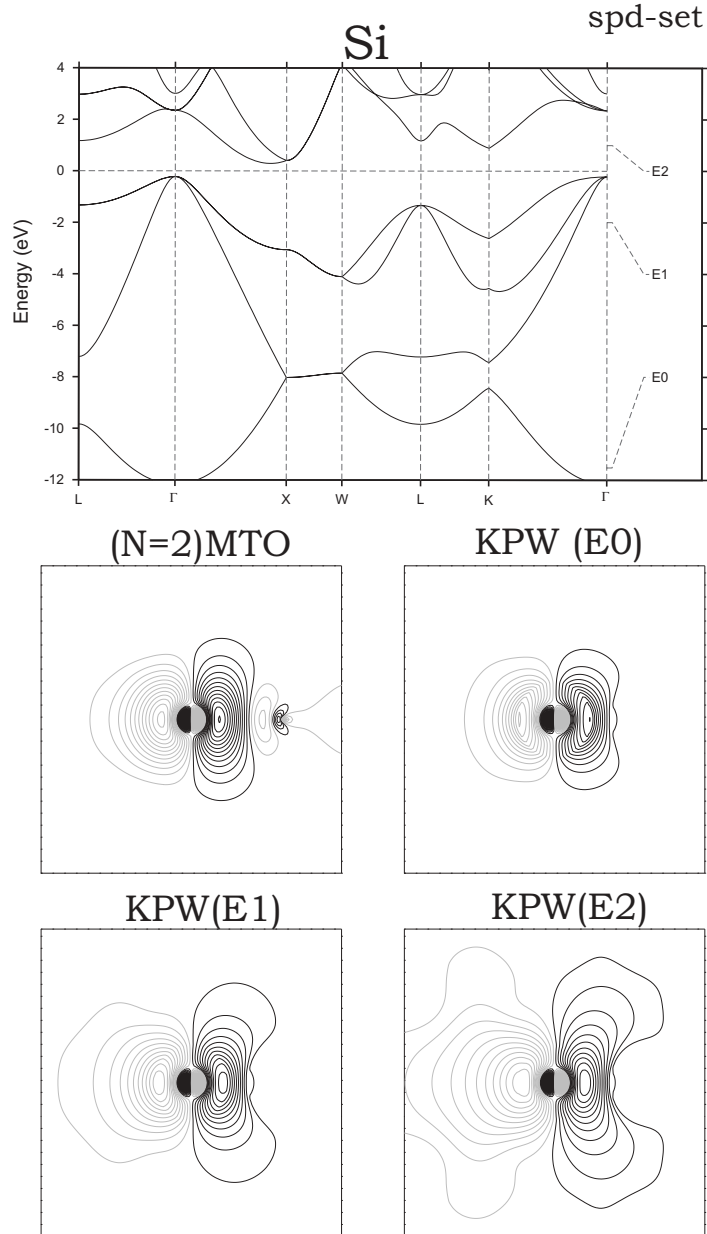


Figure 1: Band structure of Si calculated with the Si *spd*-QMTO basis set corresponding to the energy mesh shown on the right-hand side (solid lines). The contour plots show the Si p orbital pointing in the $[111]$ -direction between two nearest neighbors in the $(2\bar{1}\bar{1})$ -plane. Shown are the kinked partial waves (KPWs) at the three energies and the QMTO. The KPWs are normalized to 1, times a cubic harmonics, at the central hard sphere. The contours are the same in all plots.

site and at the three energies ϵ_0 , ϵ_1 , and ϵ_2 . In figure 2 we show this p_{111} -QMTO, together with the p_{111} -KPW at the three energies, along the line connecting the two nearest neighbors and proceeding into the back-bond.

In general, the members (labelled by $R'L'$) of the NMTO basis set for the energy mesh $\epsilon_0, \dots, \epsilon_N$ are superpositions,

$$\chi_{R'L'}^{(N)}(\mathbf{r}) = \sum_{n=0}^N \sum_{RL \in A} \phi_{RL}(\epsilon_n, \mathbf{r}) L_{nRL, R'L'}^{(N)}, \quad (1)$$

of the kinked partial waves, $\phi_{RL}(\epsilon, \mathbf{r})$, at the $N+1$ points (labelled by n) of the energy mesh. In the present case, the L -summation is over the nine s -, p -, and d -KPWs, and the R -summation is over all Si sites. Due to the localized nature of the KPWs illustrated in the figures, the latter summation is limited to the neighbors. The RL -values for which we have MTOs in the basis set, we label *active* (A), or low. Expression (1) is the energy-quantized form of Lagrange interpolation,

$$\chi^{(N)}(\epsilon) \approx \sum_{n=0}^N \phi(\epsilon_n) l_n^{(N)}(\epsilon), \quad l_n^{(N)}(\epsilon) \equiv \prod_{m=0, \neq n}^N \frac{\epsilon - \epsilon_m}{\epsilon_n - \epsilon_m},$$

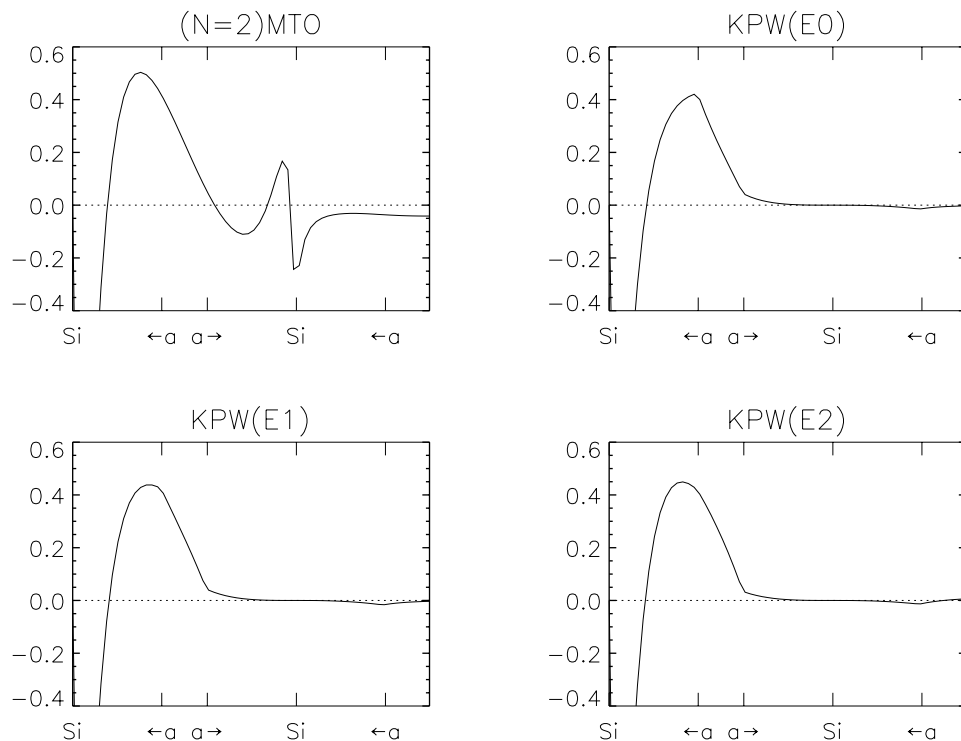


Figure 2: Si p_{111} -KPW for the Si spd -set plotted along the $[111]$ -line connecting nearest neighbors. The a 's indicate the hard spheres at the central and the nearest-neighbor sites. The generating MT-potential had no repulsive potential wells at interstitial sites (E), but only large Si-centered wells with $s = 1.7a$.

of a function of energy, $\phi(\varepsilon)$, by an N th-degree polynomial, $\chi^{(N)}(\varepsilon)$: The N th-degree polynomial, $l_n^{(N)}(\varepsilon)$, is substituted by a matrix with elements, $L_{nRL,R'L'}^{(N)}$, the function of energy, $\phi(\varepsilon)$, by a Hilbert space with axes, $\phi_{RL}(\varepsilon, \mathbf{r})$, and the interpolating polynomial, $\chi^{(N)}(\varepsilon)$, by a Hilbert space with axes, $\chi_{R'L'}^{(N)}(\mathbf{r})$.

As illustrated in figures 1 and 2, a kinked partial wave is basically a partial wave with a tail joined continuously to it with a *kink* at a central, so-called hard sphere of radius a_R . This kink is seen most clearly for the lowest energy, ε_0 . As usual, the partial wave is $\varphi_{RI}(\varepsilon, r) Y_L(\hat{\mathbf{r}}_R)$, where the function of energy is the regular solution of the radial Schrödinger equation,

$$- [r\varphi_{RI}(\varepsilon, r)]'' = [\varepsilon - v_R(r) - l(l+1)/r^2] r\varphi_{RI}(\varepsilon, r), \quad (2)$$

for the potential-well $v_R(r)$. The tail of the kinked partial wave is a so-called *screened spherical wave*, $\psi_{RL}(\varepsilon, \mathbf{r})$, which is essentially the solution with energy ε of the wave equation in the interstitial between the hard spheres, $-\Delta\psi(\varepsilon, \mathbf{r}) = \varepsilon\psi(\varepsilon, \mathbf{r})$, with the boundary condition that, independent of the energy, $\psi_{RL}(\varepsilon, \mathbf{r})$ go to $Y_L(\hat{\mathbf{r}}_R)$ at the central hard sphere, and to *zero* (with a kink) at all other hard spheres. It is this latter *confinement*, easily recognized in the plots, particularly at the highest energy ε_2 , which makes the screened spherical waves, the KPWs, and the MTOs localized when the energy is not too high. At the same time, it makes the KPW have pure L -character merely at its central sphere, because outside, it is influenced by the hard spheres centered at the neighbors. The default value of the hard-sphere radii, a_R , is 90 per cent of the appropriate covalent, atomic, or ionic radius. The kinked partial wave thus has a kink, not only at its own, but also at the neighboring hard spheres, inside which it essentially vanishes. 'Essentially' because the above-mentioned boundary condition only applies to the active components of the spherical-harmonics expansions of the screened spherical wave on the hard spheres. For the remaining components, in the present case the Si f - and higher components, as well as all components on empty (E) spheres, the screened spherical wave equals the corresponding partial-wave solution of Schrödinger's equation throughout the MT-sphere. The small bump seen in figure 1 in the lowest KPW contour along the [111]-direction is mainly caused by the f -character on the nearest neighbor, and so is the finite amplitude seen in figure 2 inside the nearest hard sphere.

3 Computational steps

The radial Schrödinger (Dirac) equations (2) are integrated numerically from $r = 0$ to s_R . This yields the radial functions, $\varphi_{RI}(\varepsilon, r)$, and their phase shifts, $\eta_{RI}(\varepsilon)$, each of which are obtained by matching the logarithmic derivative of $\varphi_{RI}(\varepsilon, r)$ at $r = s_R$ to that of

$$\varphi_{RI}^o(\varepsilon, r) \propto j_l(\kappa r) - \tan \eta_{RI}(\varepsilon) n_l(\kappa r). \quad (3)$$

The radial integration must be performed for each potential well and for each l , increasing until all further phase shifts vanish due to dominance of the centrifugal term in (2).

The screened spherical waves are specified by a Hermitian structure matrix, whose element $B_{R'L',RL}(\varepsilon)$ is essentially the radial logarithmic derivative of the L' -component in the spherical-harmonics expansion at the hard sphere at site R' of the screened spherical wave $\psi_{RL}(\varepsilon, \mathbf{r})$. What is known analytically, is the element

$$B_{R'L',RL}^0(\varepsilon) \equiv \sum_{l''} 4\pi i^{-l+l''-l''} C_{LL'l''\kappa n_{l''}}(\kappa|\mathbf{R}-\mathbf{R}'|) Y_{L''}^*(\widehat{\mathbf{R}-\mathbf{R}'}),$$

of the *bare* KKR structure matrix, which specifies how the spherical wave, $n_l(\kappa r_R) Y_L(\hat{\mathbf{r}}_R)$, at site R is expanded around another site, R' , in regular spherical waves, $j_{l'}(\kappa r_{R'}) Y_{l'}(\hat{\mathbf{r}}_{R'})$. Here

$\kappa^2 \equiv \varepsilon$, and the on-site terms of the bare structure matrix are defined to vanish. Screening of the structure matrix,

$$\left[B(\varepsilon)^{-1} \right]_{RL,R'L'} \equiv \left[B^0(\varepsilon)^{-1} \right]_{RL,R'L'} + \kappa^{-1} \tan \alpha_{RL}(\varepsilon) \delta_{RR'} \delta_{LL'},$$

requires inversion of the matrix $B_{RL,R'L'}^0(\varepsilon) + \kappa \cot \alpha_{RL}(\varepsilon) \delta_{RR'} \delta_{LL'}$. This can be done by fixing R and limiting R' to the 10-50 nearest sites. $\alpha_{RL}(\varepsilon)$ are the hard-sphere phase shifts for the active channels,

$$\tan \alpha_{RL}(\varepsilon) \equiv j_l(\kappa a_R) / n_l(\kappa a_R),$$

and, for the remaining channels, $\alpha_{RL}(\varepsilon)$ are the proper phase shifts, $\eta_{RL}(\varepsilon)$. The latter channels, which will not have KPWs and MTOs associated with them, are said to be *downfolded*. With appropriate division into active and downfolded channels, the screened structure matrix will have short spatial range and no poles in the energy-range of the occupied states.

A kinked partial wave is defined as:

$$\phi_{RL}(\varepsilon, \mathbf{r}) = [\varphi_{RL}(\varepsilon, r_R) - \varphi_{RL}^o(\varepsilon, r_R)] Y_L(\hat{r}_R) + \psi_{RL}(\varepsilon, \mathbf{r}), \quad (4)$$

where $\varphi(\varepsilon, r)$ is the radial solution for the central well from 0 to s , and $\varphi^o(\varepsilon, r)$ is the phase-shifted wave (3) proceeding smoothly *inwards* from s to the central a -sphere, where it is matched with a kink to the screened spherical wave $\psi(\varepsilon, \mathbf{r})$. The kinks of the KPW set are then given by the kink matrix,

$$K_{RL,R'L'}(\varepsilon) \equiv \frac{B_{RL,R'L'}(\varepsilon) + \kappa \cot \eta_{RL}^\alpha(\varepsilon) \delta_{RR'} \delta_{LL'}}{-\varepsilon n_l(\kappa a_R) n_{l'}(\kappa a_{R'})}, \quad (5)$$

where $\eta_{RL}^\alpha(\varepsilon)$ is the phase shift with respect to the hard-sphere medium,

$$\tan \eta_{RL}^\alpha(\varepsilon) \equiv \tan \eta_{RL}(\varepsilon) - \tan \alpha_{RL}(\varepsilon).$$

The rows and columns of the kink matrix run merely over active channels. In the formalism above, we have for simplicity used the notation of scattering theory, which is analytical for $\varepsilon > 0$, and for $\varepsilon < 0$. *Screened* scattering theory with the normalization (5) is however analytical in a region of interest *around* $\varepsilon = 0$.

Finally, the Lagrange matrix which gives the MTO set (1) in terms of the KPW set (4), is given solely in terms of the values of the Green matrix, $G(\varepsilon) \equiv K(\varepsilon)^{-1}$, on the energy mesh $\varepsilon = \varepsilon_0, \varepsilon_1, \dots, \varepsilon_N$. The Hamiltonian and overlap matrices in the MTO representation are given in terms of the same values of the Green matrix, plus the values of its first energy derivative, $\dot{G}(\varepsilon)$.

4 Further downfoldings

In the valence and lowest conduction bands of Si, there are only s - and p -, but no d -electrons. To describe these bands, we should therefore be able to use a basis with only Si s - and p -MTOs, that is, with only 4 orbitals per atom. We thus let the Si s - and p -partial waves remain active, while the Si d -waves are now included among the passive ones, *i.e.* those 'folded down' into the tails of the screened-spherical waves in (4). The results for the bands and the p_{111} -QMTO are shown in figures 3 and 4. These bands are indistinguishable from those obtained with the Si spd -set, on the scale of the figure, although between the energies of the mesh, the former bands do lie slightly above the latter. However, by making the mesh denser (increasing N), the accuracy can be increased arbitrarily. The KPW of the sp -set is seen to have d -character on the

nearest Si neighbor, and the QMTO and the KPW, particularly the one at the highest energy, are seen to be somewhat less localized than those for the *spd*-set.

It is even possible to construct an arbitrarily accurate MTO-basis which spans merely the *occupied* orbitals, that is, which spans the valence band with a basis of merely 2 orbitals per atom. For tetrahedrally coordinated covalent semiconductors like Si, it is customary to take the valence-band orbitals as the bond-orbitals, which are the bonding linear combinations of directed sp^3 -hybrids of orthonormal orbitals. It is, however, far simpler and more general, *e.g.* not limited to elemental semiconductors and tetrahedral structures, to take the valence-band orbitals as the *s*- and *p*-MTOs on *every second* Si atom, all partial waves on the nearest neighbors being

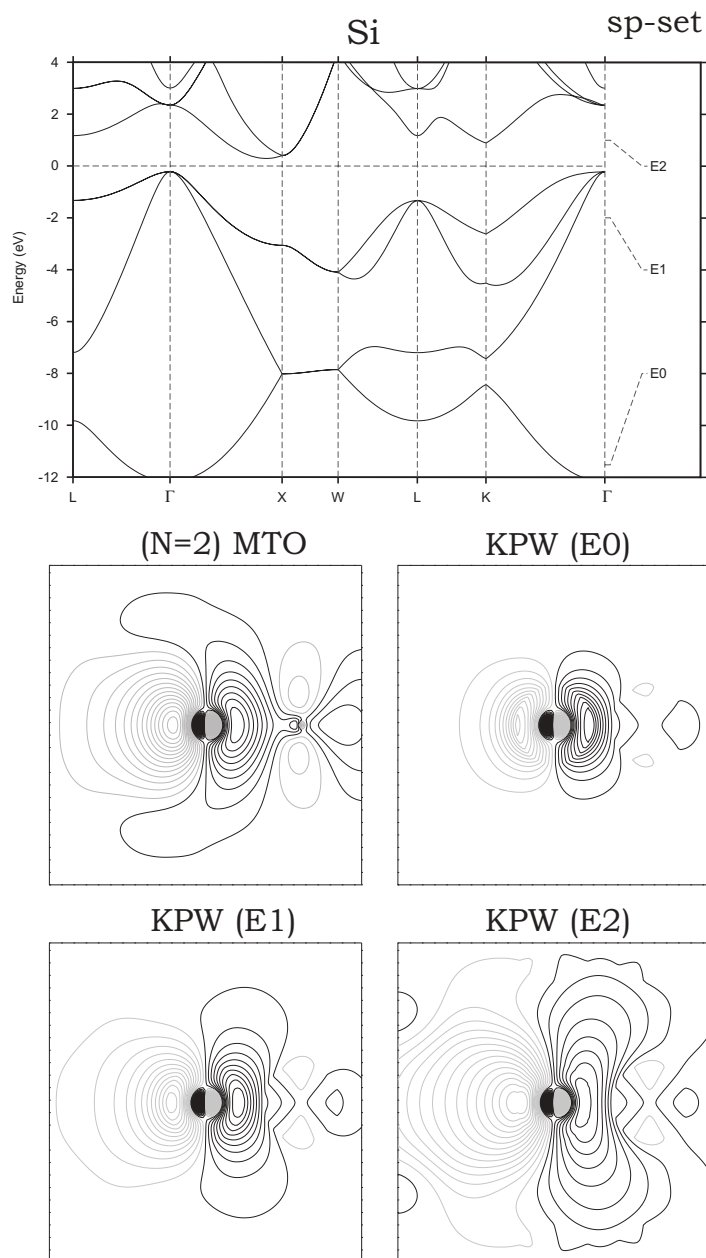


Figure 3: Same as figure 1, but for the Si *sp*-set.

downfolded. This corresponds to a $\text{Si}^{4+}\text{Si}^{4-}$ ionic picture. This QMTO-set turns out to describe merely the valence band, and to do so surprisingly well considering the fact that the two silicons are treated differently, so that the degeneracy along the XW-line is, in fact, slightly broken. The error between the energy points is proportional to $[\varepsilon_i(\mathbf{k}) - \epsilon_0][\varepsilon_i(\mathbf{k}) - \epsilon_1][\varepsilon_i(\mathbf{k}) - \epsilon_2]$, exactly as for the basis with 4 orbitals per atom shown in figure 3, because we use QMTOs in both cases, but the prefactors are larger for the smaller basis: As the number of active channels decreases, the KPWs attain longer range and stronger energy dependence. However, by making the energy mesh finer, the errors of the MTO set can be made arbitrarily small. In the bottom line of figure 5, we show the result of such a valence-band-only calculation with $N = 3$ for Ge, together with the p_{111} cubic MTO (CMTO) centered on the Ge atom to the right. The accuracy of the valence band is superb, and the MTO is seen to spill over onto the nearest-neighbor atom(s) which were chosen not to have orbitals associated with them.

Since this basis is *complete* for the *occupied* states, we may compute the density-functional ground-state properties in *real space* by taking traces, provided that we first Löwdin orthonormalize the basis in real space. The sum of the one-electron energies is then computed as the trace of the Hamiltonian, *i.e.* as the sum of the energies of the orthonormal orbitals, and the charge density is computed as the sum of the squares of these orbitals. This is a method where the amount of computation increases merely linearly with the size of the system, a so-called *order- \mathcal{N} method*. Here, \mathcal{N} refers to the number of atoms in the system and not to the order N of the MTOs. This NMTO method, which generates the complete basis for the occupied states

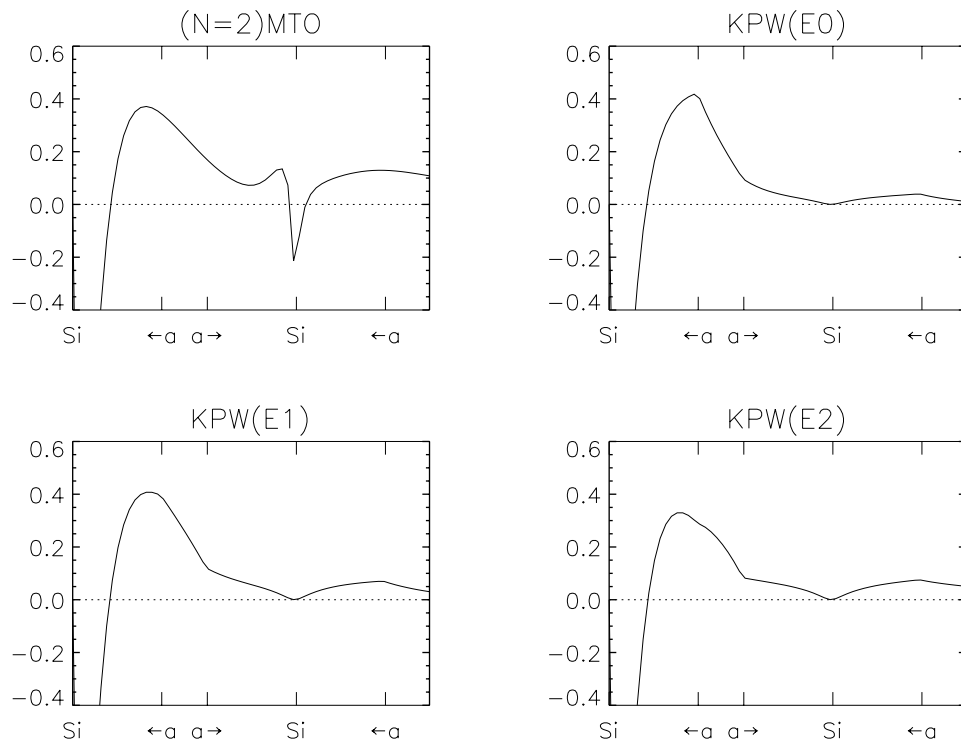


Figure 4: Same as figure 2, but for the Si *sp*-set.

a priori, should be superior to current order- \mathcal{N} methods, which either use inaccurate empirical tight-binding models or project onto the occupied states during the course of a large-basis-set calculation.

In order to demonstrate in further detail that our method works, we consider Si in the diamond structure for which the valence-band Wannier functions can be taken as *bond orbitals*.

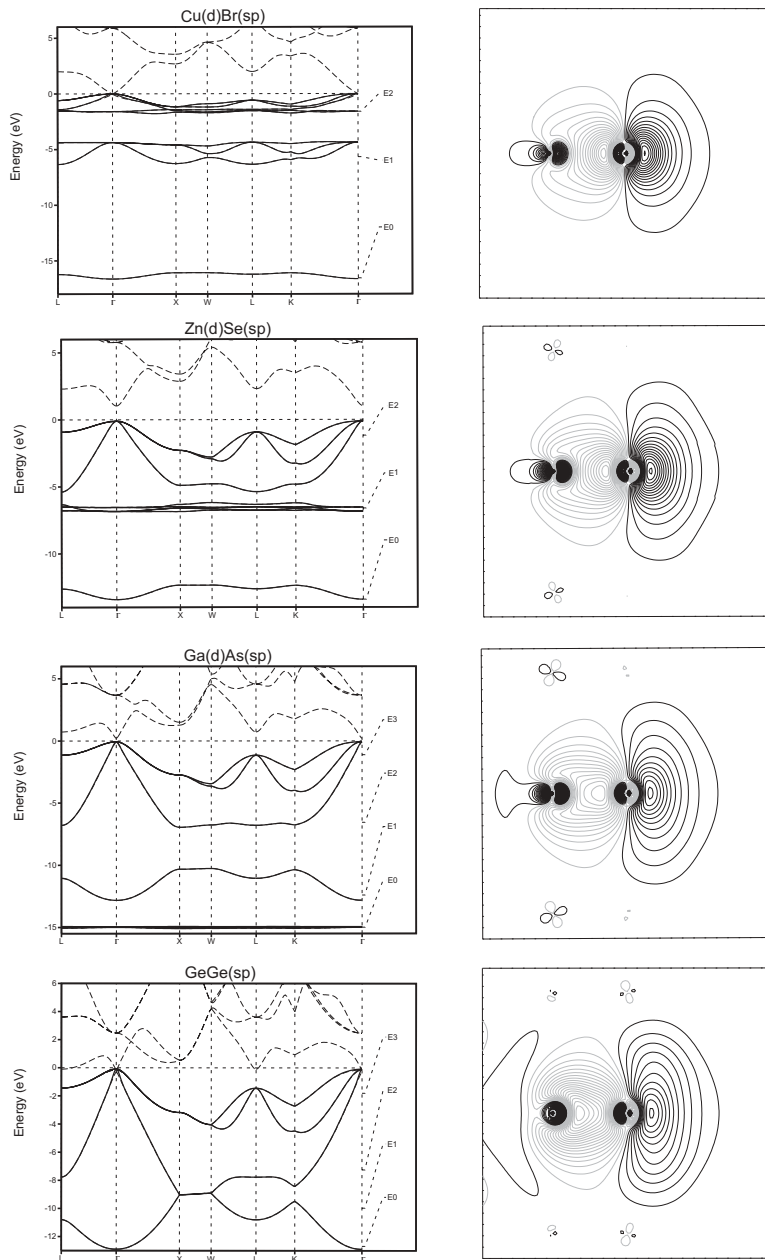


Figure 5: Valence bands (solid lines) of the series CuBr – Ge, calculated with the ionic basis sets where the *sp*-MTOs are on the anion and, except for Ge, the *d*-MTOs are on the cation. The exact bands are given by dashed lines. The contour plots show the p_{111} -MTO on the anion (the atom to the right). The ionicity decreases and the covalency increases from the top to the bottom.

First, we orthonormalize our symmetry-breaking Si^{4+} s, p_x, p_y, p_z QMTO set. The resulting $\text{Si } s$ and $\text{Si } p_x$ orbitals are shown in the $(1\bar{1}0)$ -plane in figures 6 and 7. These orthogonalized orbitals are seen to remain fairly localized. Then, we transform to the four congruent sp^3 -hybrids centered nominally on every second Si atom. As figure 8 shows, such an sp^3 -hybrid is, in fact,

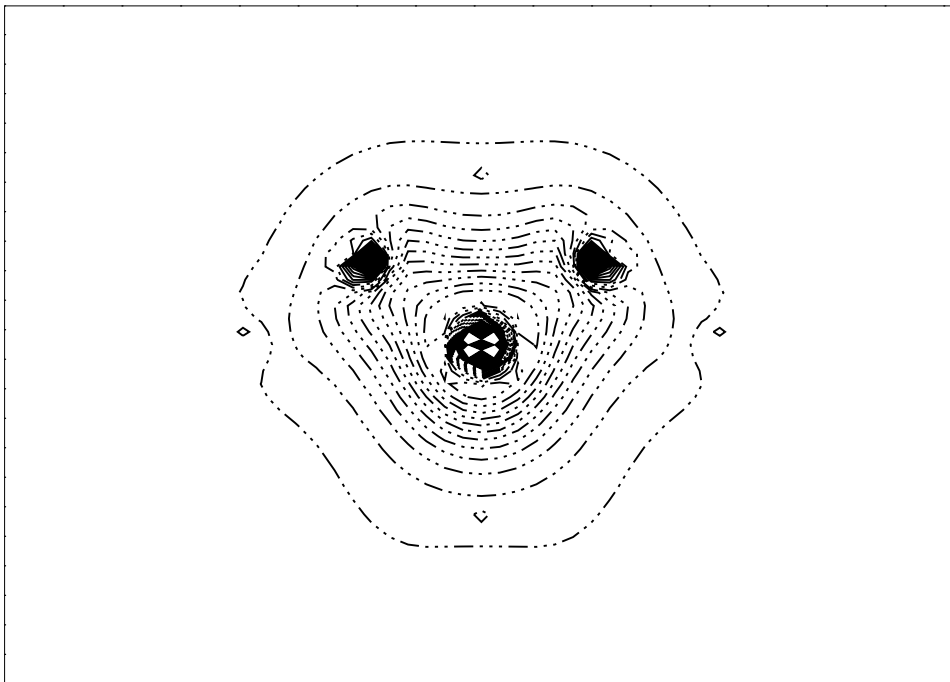


Figure 6: Contour plot in the $(1\bar{1}0)$ -plane of the orthogonalized s -QMTO on the central Si atom. All partial waves on the nearest neighbors (and their lattice translations) were downfolded.

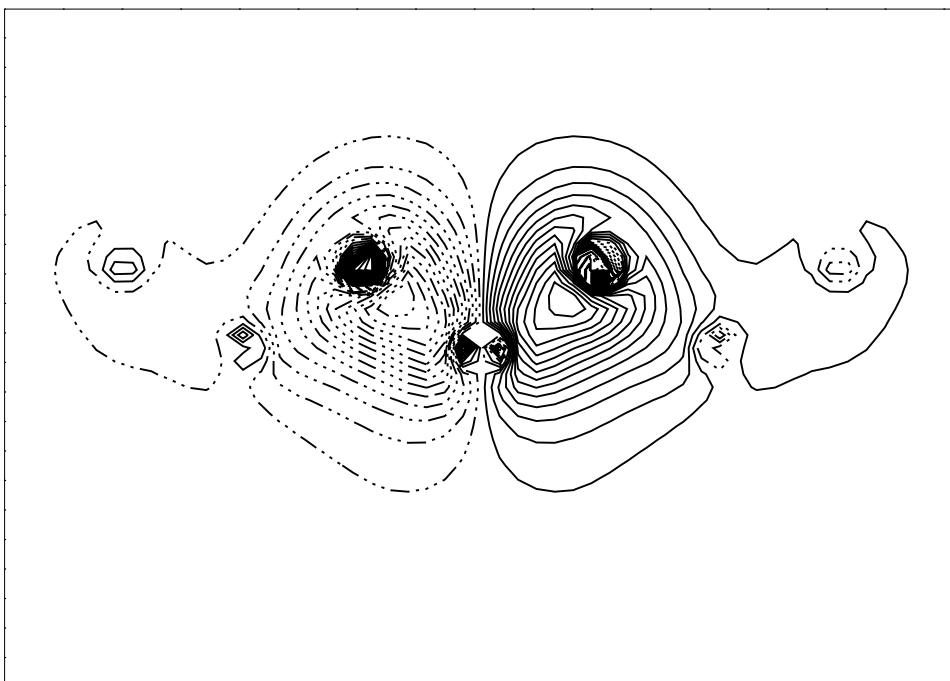


Figure 7: Same as figure 6, but for the p_x -QMTO.

the bond orbital. Hence, folding all partial waves of the atoms chosen not to carry orbitals, into the tail of the sp^3 -directed orbital on one of the other Si atoms, has made that orbital look like a bond orbital. The reason why the figure does not show exact symmetry between the two sites is caused by our use of an energy mesh with only 3 points in the valence band. Making the energy mesh finer will generate the exact symmetry.

Now, Sn is metal because the bonding and antibonding bands overlap. This should, however, not prevent our method from working for the occupied states only, because NMTOs are *energy selective*. Since the orbitals will be shaped in such a way that the basis set solves Schrödinger's equation exactly for the energies on the mesh, we may merely have to choose several energy points in the region of band overlap *below* the Fermi level –and, of course, *no* energy points above. Remember that our ionic prescription does not make use of the fact that the Wannier functions for the valence and conduction bands are respectively bonding and antibonding.

Since the ionic Si Si(sp) set gives the occupied states in diamond-structured Si with arbitrary accuracy, the same procedure with the sp -orbitals placed exclusively on the anion, and the d -orbitals on the cation, will of course work for any IV-IV, III-V, II-VI, and I-VII semiconductor and insulator. CuBr, for instance, would be thought of as an ionic compound Cu^+Br^- with the closed-shell configuration $\text{Cu}3d^{10}\text{Br}4s^24p^6$, and the basis should therefore have the d -MTOs on the Cu atoms and the s and p -MTOs on the Br atoms. This is illustrated in the upper line of figure 5. Being a single-site prescription, this works for CuBr in *any* structure. What we have seen is thus, that the MTO basis can be designed *a priori* to span the Hilbert space of the occupied states only. That is, there is one, and only one, such MTO per electron. To specify such a set, one would, in order to get the electron-count right, put the orbitals where the electrons are thought to be, and leave it to the method to *shape* the tails of these orbitals in such a way that the basis solves Schrödinger's equation exactly for occupied states of the given static mean-field (*e.g.* LDA) potential. Such *ionic MTO basis sets*, which 'automatically' span the occupied –and no further– states of any *band insulator*, could make density-functional molecular-dynamics calculations highly efficient for such systems.

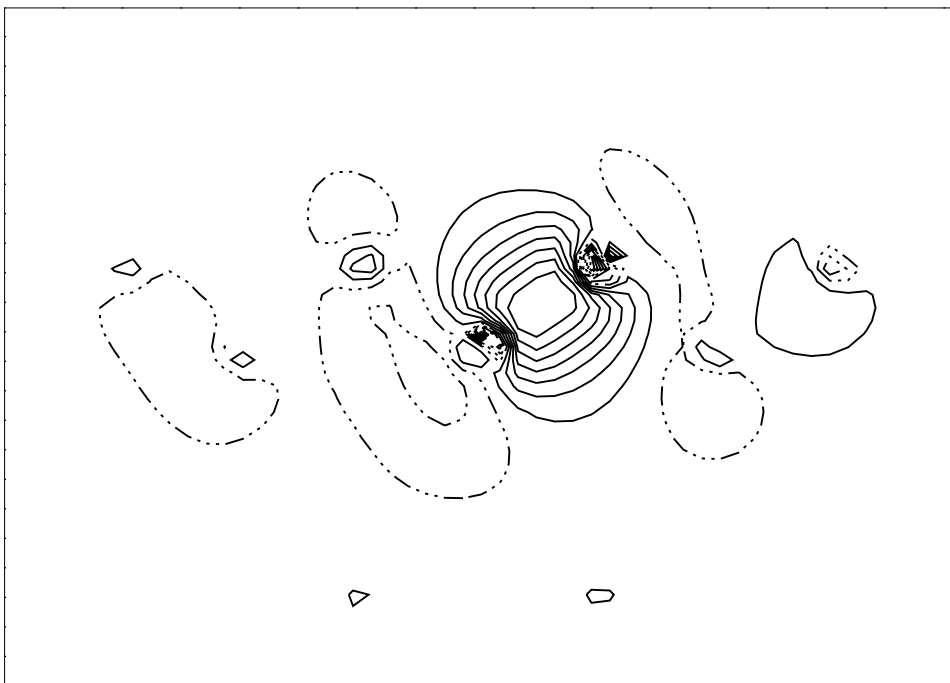


Figure 8: Same as figure 6, but for the sp^3 -hybrid. For increasing N , this orbital converges to the bond orbital.

How could one imagine to treat a chemical reaction like: $2H_2O \rightarrow 2H_2 + O_2$ with MTO bases of occupied states only? For water, it is natural to use the ionic description $H_2^+O^{--}$, according to which the orbital configuration is $O p^6$, *i.e.* one would put the p orbitals on oxygen and fold down all partial waves centered on the hydrogens. In principle, one might stick to this configuration throughout the reaction, because it keeps the electron-count right. However, the oxygen-centered orbitals would eventually look strange and have long range, because they would have to separate off pieces of wave functions sitting on the hydrogens. Such oxygen orbitals might be more time-consuming to generate. At some stage in the reaction, it might therefore be appropriate to switch to configurations such as $Hs \uparrow Hs \downarrow$, or $H Hs^2$ for the hydrogen molecule; this is analogous to our treatment of the occupied states in tetrahedrally coordinated Si. For O_2 with the *open-shell* molecular configuration $pp\sigma^2 pp\pi^4 pp\pi \uparrow\uparrow$, we might use an 'ionic' configuration like: $O (z \uparrow x \uparrow\downarrow y \uparrow) O (z \downarrow x \uparrow y \uparrow\downarrow)$ with z referring to the *local* z -direction of the molecule.

This example immediately leads to a treatment of *open-shell* systems by means of spin and possibly orbital polarizations. We have seen that the 3rd-generation MTO method offers the possibility of designing single-electron bases of atom-centered localized orbitals, which span the wave functions in a given energy region of a given mean-field potential. These orbitals can even be *symmetry-breaking*, as in the case of diamond, Si, Ge, and Sn, without the generating mean field having to be so. These orbitals thus seem to have great potential in the design of *many-electron wave functions* which describe *correlated electron* systems in a *realistic* way.

5 Conclusion

We have solved the long-standing problem of deriving energy-independent, short-ranged orbitals from scattering theory (Hubbard 1967). The present formalism contains exactly the right 'physics and chemistry,' we feel. This should give the computational method great speed and accuracy, and make it a vehicle for discovery and understanding.

6 References

- Andersen O K and Jepsen O 1984 *Phys. Rev. Lett.* **53** 2571
- Andersen O K, Postnikov A V, and Savrasov S Yu 1992 *Applications of Multiple Scattering Theory to Materials Science* eds. W H Butler, P H Dederichs, A Gonis and R L Weaver, Mat. Res. Soc. Symp. Proc. Vol. **253** (Pittsburgh: Materials Research Society) 37-70
- Andersen O K, Jepsen O, and Krier G 1994 *Lectures on Methods of Electronic Structure Calculations* eds V. Kumar, O.K. Andersen, and A. Mookerjee (Singapore: World Scientific Publishing Co) 63-124
- Andersen O K, Arcangeli C, Tank R W, Saha-Dasgupta T, Krier G, Jepsen O, and Dasgupta I 1998 *Tight-Binding Approach to Computational Materials Science* eds L Colombo, A Gonis, and P Turchi, Mat. Res. Soc. Symp. Proc. Vol. **491** (Pittsburgh: Materials Research Society) 3-34
- Andersen O K, Saha-Dasgupta T, Tank R W, Arcangeli C, Jepsen O, and Krier G 2000 *Electronic Structure and Physical Properties of Solids. The Uses of the LMTO Method* ed H Dreyse (New York: Springer Lecture Notes in Physics) 3-84
- Andersen O K and Saha-Dasgupta T 2000 *Phys. Rev. B* **62** R16 219
- Arcangeli C and Andersen O K *to be published*
- Dasgupta I *et al* 2002 *Bull Mater Sci* this issue
- Dasgupta I, Saha-Dasgupta T, Andersen O K, Pavarini E, and Jepsen O *to be published*
- Hubbard J 1967 *Proc. Phys. Soc. London* **92** 921, and references therein

- Kohn W and Rostoker J 1954 *Phys. Rev.* **94** 111
- Korotin M A, Anisimov V I, Saha-Dasgupta T, Dasgupta I 2000 *Journal of Physics: Condensed Matter* **12** 113-124
- Korringa J 1947 *Physica* **13** 392
- Müller T F A, Anisimov V, Rice T M, Dasgupta I, Saha-Dasgupta T 1998 *Phys. Rev. B* **57** R12655
- Pavarini E, Dasgupta I, Saha-Dasgupta T, Jepsen O, and Andersen O K 2001 *Phys. Rev. Lett.* **87** 047003
- Sarma D D, Mahadevan P, Saha-Dasgupta T, Ray S, and Kumar A 2000 *Phys. Rev. Lett.* **85** 2549
- Savrasov D and Andersen O K *to be published*
- Tank R W and Arcangeli C 2000 *phys. stat. sol. (b)* **217** 89-130
- Valenti R, Saha-Dasgupta T, Alvarez J V, Pozgajcic K, and Gros C 2001 *Phys. Rev. Lett.* **86**, 5381 (2001)
- Zeller R, Dederichs P H, Ujfalussy B, Szunyogh L, and Weinberger P 1995 *Phys. Rev. B* **52** 8807